Tunable supermode converters based on J_x graphene waveguide arrays with transversely linear modulation

Shuaifei Ren,[1] Bing Wang,[1,*] Chengzhi Qin,[1] Weiwei Liu,[1] Lingzhi Zheng,[1] Zhuoxiong Liu,[1] and Peixiang Lu[1,2]

[1]*School of Physics and Wuhan National Laboratory for Optoelectronics, Huazhong University of Science and Technology, Wuhan 430074, China*

[2]*Hubei Key laboratory of Optical Information and Pattern Recognition, Wuhan Institute of Technology, Wuhan 430205, China*

(Received 2 November 2023; revised 16 March 2024; accepted 19 March 2024; published 5 April 2024)

Conventional mode converters are usually based on wave-number matching in the propagation direction. This often requires applying the periodic modulation in the longitudinal orientation. Here, we propose to construct an efficient supermode converter with only transverse modulation. By linearly changing the surface conductivity of J_x graphene waveguide arrays, we build a synthetic J_x lattice with linearly varying on-site potential in the modal dimension. It turns out that each supermode can fully transfer to its corresponding symmetric partner. The conversion distance of supermodes is inversely proportional to the ramp of linear modulation. In this way, tunable supermode converters can be readily implemented by modulating the surface conductivity of graphene sheets. This study may find promising applications in developing mode converters and mode-division multiplexers utilizing plasmonic waveguide arrays.

DOI: 10.1103/PhysRevA.109.043507

I. INTRODUCTION

In the last two decades, graphene plasmonics [1,2] has received much research interest due to its unique electronic and optical properties. A monolayer graphene can support transverse magnetic (TM) polarized surface plasmon polaritons (SPPs) in the infrared region. Compared to traditional noble metals, SPPs in graphene present appealing properties such as extreme confinement, low losses, and tunability [3]. With these characteristic properties, graphene SPPs have been widely used in plasmonic waveguides at infrared frequencies. Coupled graphene sheet arrays have been used to study various optical effects, including Bloch oscillations [4], Talbot effect [5], and Anderson localization [6]. The surface conductivity of graphene can be varied by adjusting the chemical potential, which is governed by the carrier density. The carrier density is actually able to be controlled by applying bias voltage [7]. Though the propagation of plasmonic supermodes has been investigated in graphene multilayers [8], the conversion of SPP supermodes has not yet been widely studied.

Synthetic dimension has been recently attracting much research interest in many physical systems such as cold atoms [9], Weyl points [10], and photonic topological insulators [11]. The synthetic modal dimension [12] has been experimentally implemented with oscillated J_x waveguide arrays. The coupling coefficients between adjacent waveguides follow the matrix elements of the angular momentum operator J_x, resulting in equally spaced propagation constants [13]. The spatial waveguide modulation guarantees the couplings of adjacent modes. Thus, the spatial J_x lattice with spatial modulations is equivalent to a synthetic lattice in the modal dimension. With the conception of synthetic dimensions, one can manipulate optical modes more flexibly.

A uniform lattice with linear on-site potential that induces Bloch oscillation has been widely studied in many different systems such as semiconductor superlattices [14], atomic systems [15], and coupled dielectric waveguide arrays [16–18]. Optical revivals occur in an infinite Bloch lattice due to its equispaced Wannier-Stark eigenspectrum [19]. For a finite lattice with linear on-site potential, the recurrence of wave packets does not occur at the edge of the lattice since the eigenfunctions that are localized at the edge do not correspond to an eigenvalue ladder [20]. However, a finite J_x lattice can exhibit the recurrence for an edge excitation because of its overall equidistant eigenspectrum. Optical revivals [13], light transitions [21,22], and quantum state transfer [23–25] have been studied in J_x waveguide arrays. J_x lattices have very intriguing features. There have been experimental works demonstrating the applicability of such optical arrangements [26,27]. A normal J_x lattice has also been applied in the multiphoton structures to investigate multiphoton discrete fractional Fourier dynamics [28]. J_x lattices with ramp potentials have emerged in the multiple-photon states [29]. The J_x lattice with linear on-site potential still holds an equally spaced eigenspectrum. In the following contents, we shall prove that a J_x lattice with linear on-site potential in real space can construct a synthetic J_x lattice with linear on-site potential in the modal dimension, which results in the perfect transfer of supermodes.

In this work, we propose to construct a tunable supermode converter based on modulated J_x graphene waveguide arrays (GWAs). By linearly changing the surface conductivity of each graphene sheet, a synthetic lattice with linear on-site potential in the modal dimension can be readily formed

*wangbing@hust.edu.cn

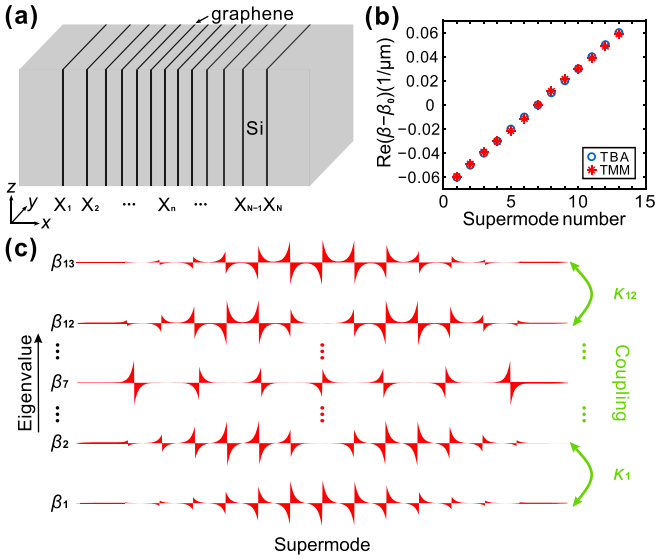

FIG. 1. (a) Schematic diagram of J_x graphene waveguide arrays. (b) Real parts of propagation constants for the spatial J_x lattice calculated in TMM and TBA method. (c) Modal ladder and profiles of supermodes.

because of the symmetric transformation matrix. In contrast to the synthetic dimension that has been constructed in Ref. [12], the modulation of our system in real space is only in the transverse direction. It results in constant coupling coefficients of supermodes in the modal dimension, which correspond to the matrix elements of J_x operator. Due to the equispaced eigenvalue spectrum, the energy of some excited supermode could efficiently transfer to its symmetric partner. Compared to traditional static mode converters, the conversion distance in our system can be conveniently adjusted by changing the surface conductivity of graphene sheets. The construction of the synthetic modal lattice provides an effective approach to manipulating the conversion of supermodes in plasmonic waveguide arrays.

II. CONSTRUCTION OF THE SYNTHETIC MODAL LATTICE

The schematic diagram of J_x GWAs is depicted in Fig. 1(a). Each monolayer graphene sheet is sandwiched between two Si layers. This structure can be constructed through a repeated process of filtering liquid-phase exfoliated graphene film and the subsequent coating of amorphous Si film via the plasma-enhanced chemical vapor deposition method [30]. The position of the graphene sheet is denoted by X_n, where n ranges 1 to N with $N = 13$ the total number of graphene waveguides. It is assumed that all graphene sheets extend infinitely in the y direction and SPPs propagate along the z direction. By controlling the thickness of Si film, the space between adjacent graphene sheets can be determined, which results in the impacts on the coupling of SPPs in graphene. The coupling coefficient between graphene waveguide n and $n+1$ is set to $C_n = (\gamma/2)[n(N-n)]^{1/2}$ to form a J_x lattice in real space, where γ is the desired difference between adjacent propagation constants of supermodes. A square root dependence on coupling constants is indeed away from a realistic situation. Actually, the coupling coefficients are determined by the distance between graphene sheets. For the J_x waveguide arrays with designed coupling constants C_n, the corresponding distance d_n can be calculated numerically. Although it is impossible to achieve irrational values for coupling coefficients, the distances are rational numbers. A small variation of distance or coupling constants could not produce a new effect. The separation of graphene sheets gradually increases from the center to the sides. Due to the presence of propagation loss in graphene, the coupling coefficients of adjacent graphene waveguides are complex numbers. Based on the transfer matrix method (TMM), we can derive the complex propagation constants of the waveguide arrays [31–33]. We first focus on the wave packet dynamics in GWAs and omit the propagation loss of SPPs in graphene. Consequently, the imaginary parts of C_n could be neglected in the analysis. The SPP modes are bounded at the positions of the graphene sheets. Thus, a tight binding approximation (TBA) can be employed. Together with nearest-neighbors approximation, the evolution of electromagnetic wave in the spatial J_x lattice can be written in the Dirac vector notation as $-id|a\rangle/dz = H|a\rangle$, where $|a\rangle = (a_1, a_2 \ldots a_n, \ldots, a_N)^T$, a_n denotes the complex field amplitude in graphene waveguide n, and H is the Hamiltonian of the system. The matrix elements of H are given by $H_{m,n} = (\delta_{m-1,n} + \delta_{m+1,n})C_n$, where $\delta_{m-1,n}$ and $\delta_{m+1,n}$ are Kronecker deltas. Since H is a real Hermitian matrix, it has a complete set of real orthonormal eigenvectors (supermodes) with real eigenvalues. By solving the eigenvalue equation $H|a\rangle = \beta|a\rangle$ we can obtain the supermode eigenvalues $\beta_i = [i - (N+1)/2]\gamma (i = 1, 2, \ldots, N)$ and corresponding eigenvectors $|a^{(i)}\rangle$, where the superscript i denotes the order of the supermode. Here, the supermodes are sorted in ascending order of eigenvalues. The propagation constants of the supermodes $(\beta_0 + \beta_i)$ are equally spaced, where β_0 is the propagation constant of the individual graphene waveguide. As a comparison, we calculate the propagation constants using TMM to measure the accuracy of the TBA method. The results as shown in Fig. 1(b) are obviously convincing. The magnetic field component H_y of each supermode can be expressed as the superposition of TM modes in all graphene waveguides $\psi_i(x) = \Sigma_n a_n^{(i)} \phi_n(x)$, where $\phi_n(x)$ is the magnetic field distribution in the graphene waveguide n. The supermode ladders and corresponding field distribution are depicted in Fig. 1(c). The equally spaced propagation constants of supermodes and their adjacent coupling could form a synthetic lattice in the modal dimension.

The eigenmodes of the spatial J_x lattice form an equally spaced ladder in the synthetic modal dimension, but they are orthogonal to each other. To couple the supermodes, we vary the surface conductivity of graphene sheets along their transverse direction. The amplitude of the variation is linearly increasing. Let us assume that the variation is expressed as a perturbation $H'_{m,n} = \alpha\delta_{m,n}\beta_n$ in the Hamiltonian matrix, where α is the proportion of perturbations to the eigenvalues of unperturbed spatial J_x lattice. There is a real orthogonal matrix Q which transforms the unperturbed Hamiltonian to a diagonal matrix $\Lambda = Q^T H Q$, whose diagonal elements are eigenvalues of all supermodes, that is to say $\Lambda_{m,n} = \delta_{m,n}\beta_n$. Thus, the perturbation can be denoted as $H' = \alpha\Lambda$. The

Hamiltonian matrix with perturbation in real space is

$$H + H' = \begin{bmatrix} \alpha\beta_1 & C_1 & 0 & \cdots & 0 \\ C_1 & \alpha\beta_2 & C_2 & \cdots & 0 \\ 0 & C_2 & \alpha\beta_3 & \cdots & \vdots \\ \vdots & \vdots & \vdots & \ddots & C_{N-1} \\ 0 & 0 & \cdots & C_{N-1} & \alpha\beta_N \end{bmatrix}. \quad (1)$$

According to perturbation theory, we derive the new Hamiltonian $\Lambda' = Q^{\mathrm{T}}(H + H')Q$ in modal space by applying the representation transformation. Since the transformation matrix Q is a real symmetric matrix [13], namely $Q^{\mathrm{T}} = Q$, we can obtain the Hamiltonian $\Lambda' = \Lambda + \alpha H$ in the modal dimension. Thus, the Hamiltonian matrix in modal space is

$$\Lambda' = \begin{bmatrix} \beta_1 & \alpha C_1 & 0 & \cdots & 0 \\ \alpha C_1 & \beta_2 & \alpha C_2 & \cdots & 0 \\ 0 & \alpha C_2 & \beta_3 & \cdots & \vdots \\ \vdots & \vdots & \vdots & \ddots & \alpha C_{N-1} \\ 0 & 0 & \cdots & \alpha C_{N-1} & \beta_N \end{bmatrix}. \quad (2)$$

Here, the linear on-site potential in the modal dimension is introduced and they are exactly equal to the eigenvalues of supermodes in real space. Particularly, the second item αH indicates that adjacent supermodes couple to each other. The coupling coefficients are proportional to the coupling between adjacent graphene waveguides in real space. It means that a J_x lattice with linearly on-site potential in the modal dimension is formed. For a J_x lattice in real space without modulation, supermodes are orthogonal to each other. As a result, a given eigenmode should propagate without any deformation. The additional modulation causes the coupling of supermodes for the original J_x lattice in real space. Then we consider the dynamics of supermodes for the origin J_x lattice without additional modulation. For an arbitrary incident wave packet $\Psi(x, 0) = \Sigma_n b_n(0)\psi_n(x)$, the magnetic field distribution at the propagation distance z could be expressed as the superposition of all supermodes $\Psi(x, z) = \Sigma_n b_n(z)\psi_n(x)\exp(i\beta_n z)$. As a result, we can get the complex amplitude of the nth supermode at any distance by utilizing the orthogonality relations of the different supermodes, which is $b_n(z) = \int \psi_n(x)\exp(-i\beta_n z)\Psi(x, z)dx$. Then, the conversion of supermodes can be readily analyzed by calculating the modal intensity $|b_n(z)|^2$.

III. CONVERSION OF SUPERMODES

The supermode conversions can be analyzed by numerical simulation of the wave packets in modulated graphene waveguide arrays. The parameters used here should be rational and consistent with those extracted from real materials. The details of getting the parameters can be found in past works about SPPs in graphene [34–36]. In our study, the wavelength of the incident wave packets is set to $\lambda = 10$ μm ($\hbar\omega = 0.124$ eV). We consider the graphene sheet with chemical potential $\mu_c = 0.8$ eV. The corresponding relaxation time is $\tau = 0.8$ ps. The difference between adjacent propagation constants of supermodes is set to $\gamma = 0.01\ \mu\mathrm{m}^{-1}$. The propagation constant of SPPs for a single graphene waveguide has a relation to the surface conductivity as $\beta_0 = k_0[1 - 2\varepsilon_d/(Z_0\sigma_g)]^{1/2}$, where $k_0 = 2\pi/\lambda$ is the incident wavelength number, ε_d is the relative permittivity of the filling dielectric medium, Z_0 is the impedance of free space. We modulate the surface conductivity of graphene sheets along the x direction as $\Delta\sigma_g(n) = \{[n - (N + 1)/2]\delta\}\sigma_{g0}$ in simulation, where σ_{g0} is the basic surface conductivity without perturbation and δ is the linear ramp of modulation amplitude. As a consequence, the variation of propagation constants for the graphene waveguide n is $\Delta\beta(n) \approx -[n - (N + 1)/2]\delta\beta_0$. The ramp of modulation amplitude for surface conductivity of graphene sheets is set to $\delta = 0.005$. The variation is small enough so that it can be regarded as a perturbation for the Hamiltonian in real space. The perturbation is expressed as $H'_{m,n} = \delta_{m,n}[n - (N + 1)/2]\delta\beta_0$ in Hamiltonian matrix. Compared with the form $H'_{m,n} = \delta_{m,n}[n - (N + 1)/2]\alpha\gamma$ that has been assumed above, the relation $\alpha\gamma = \delta\beta_0$ can be acquired. As discussed above, the elements of the Hamiltonian matrix Λ' in modal space are given by $\Lambda'_{m,n} = \delta_{m,n}\beta_n + (\delta_{m-1,n} + \delta_{m+1,n})\kappa_n$, where $\kappa_n = (\delta\beta_0/2)[n(N-n)]^{1/2}$ is the coupling coefficient between the nth and $(n + 1)$th supermode and γ is the linear ramp of on-site potential in this synthetic lattice. The eigenvalues of the Hamiltonian matrix Λ' in the modal dimension are still equispaced. It results in field recovery with the period $2L = 2\pi/\gamma'$, where $\gamma' = [\gamma^2 + (\delta\beta_0)^2]^{1/2}$ is the spacing of propagation constants in this system. The ramp of propagation constants γ for the spatial J_x lattice is equivalent to the ramp of on-site potential in the modal dimension. The product of the modulation ramp δ for surface conductivity and the propagation constants β_0 for a single graphene waveguide indicates the coupling strength between adjacent supermodes in modal space. Typically, there are efficient conversions of energy between symmetric orders of supermodes at the conversion distance $z = L$ [21]. Figures 2(a)–2(c) show the distribution of field intensity in real space for a single incidence of the first, fourth, and tenth supermode in transversely modulated J_x graphene waveguide arrays. The field intensity does not evolve obviously. However, the corresponding phase distributions as shown in Figs. 2(d)–2(f) do vary evidently. In Figs. 2(g)–2(i), we show the dynamics of the synthetic lattice in modal space for a certain supermode excitation. As displayed in Fig. 2(g), when the first supermode is excited, it will couple to higher supermodes until it transfers to the highest supermode at the conversion distance. The transformation rate $|b_{13}(L)|^2$ can achieve up to 0.98. In Fig. 2(h), if the fourth supermode is launched, it will convert to the tenth supermode and vice versa as depicted in Fig. 2(i). Here, the lowest and the highest supermodes act as the boundaries of the synthetic modal lattice. In a word, if the nth supermode is launched, it couples to both lower and higher supermodes and transfers to the symmetric $(N + 1 - n)$th supermode. It can be seen that the supermode transfers to the desired mode at the conversion distance as expected in spite of the overall loss in graphene sheets. From the expression of conversion distance $L = \pi/[\gamma^2 + (\delta\beta_0)^2]^{1/2}$, we learn that the conversion distance is determined by the difference between adjacent propagation constants of spatial J_x lattice, the modulation ramp of the surface conductivity of graphene, and the propagation constants of a single graphene waveguide. The surface conductivity is able to be changed by varying the applied gate voltage on

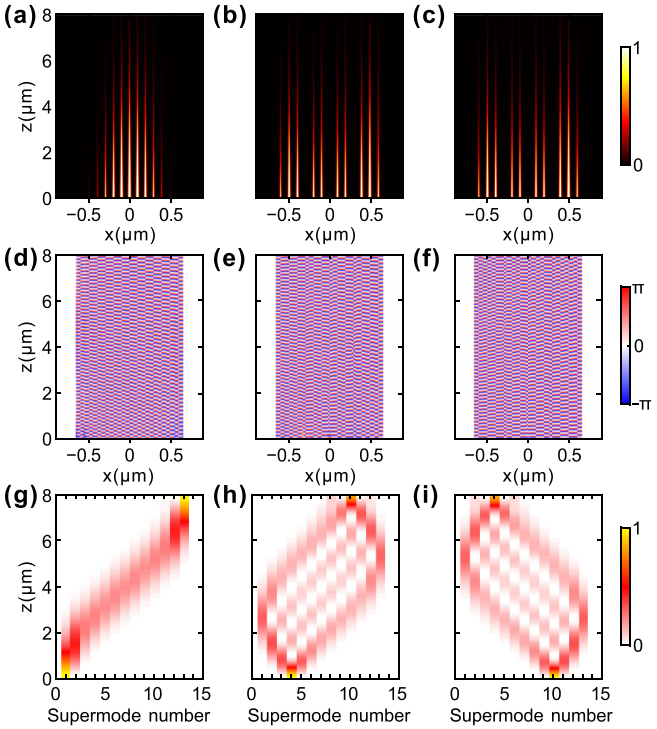

FIG. 2. (a)–(c) Distribution of field intensity in real space for a single incidence of first, fourth, and tenth supermode in transversely modulated J_x graphene waveguide arrays. (d)–(f) Corresponding phase distribution for (a)–(c). (g)–(i) Evolution of the normalized intensity for supermodes in the modal dimension.

graphene. Thus, the conversion distance of supermodes in graphene waveguide arrays can be conveniently modulated.

IV. EFFECT OF MODULATION PARAMETERS

With the excitation of the fundamental supermode, we investigate the relation between the conversion distance and the modulation ramp by analyzing the dynamics in modal space. Figure 3(a) shows the numerical results of the relationship between L and δ with the incident wavelength $\lambda = 8$, 10, and 12 μm. It can be known that the conversion distance decreases as the modulation ramp increases at a fixed incident wavelength, which coincides with the analytical results cal-

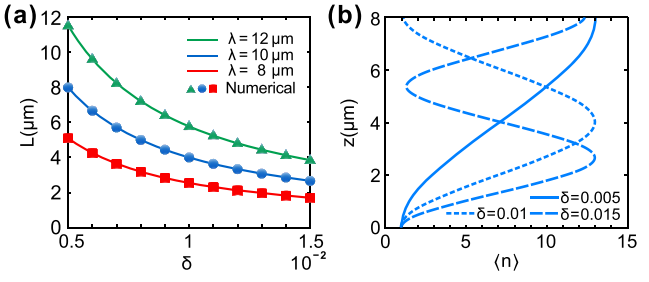

FIG. 3. (a) Relation between γ and the conversion distance L obtained by simulation data and TBA method with the incident wavelength $\lambda = 8$, 10, 12 μm. (b) Tracks of average modal intensity in modal space for $\delta = 0.005$, 0.01, and 0.015 with the excitation of fundamental mode at $\lambda = 10$ μm.

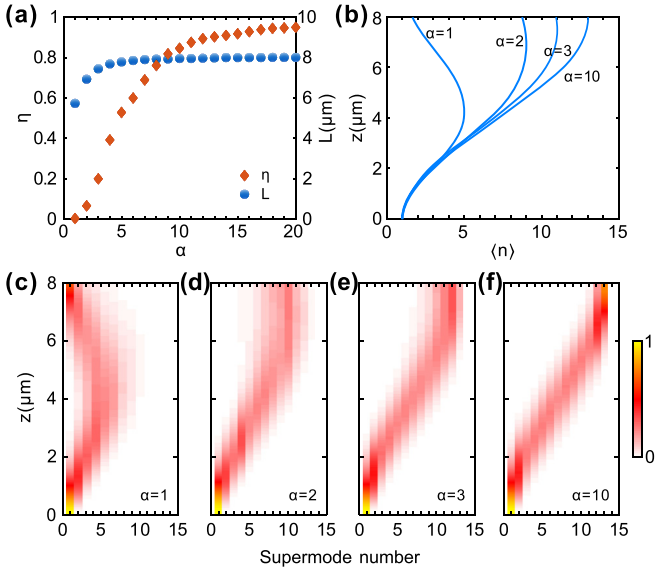

FIG. 4. (a) Conversion distance and the transformation rate versus the perturbation coefficient. (b) Tracks of average modal intensity in modal space for $\alpha = 1$, 2, 3, and 10 with the excitation of fundamental supermode at $\lambda = 10$ μm. (c)–(f) Corresponding dynamics of supermodes in modal space for the tracks in (b).

culated by the equation of conversion distance. In addition, the conversion distance is more sensitive to the modulation ramp at higher incident wavelength. For a constant modulation ramp, the conversion distance increases with the incident wavelength. The mean of modal intensity in synthetic space is defined as $\langle n \rangle(z) = \Sigma_n n|b_n(z)|^2$. In Fig. 3(b), we display the tracks of average modal intensity for $\delta = 0.005$, 0.01, and 0.015 with the excitation of fundamental supermode at $\lambda = 10$ μm. It clearly shows that the modulation ramp can determine the conversion distance of supermodes in this system. It is worth noting that the linearly increasing on-site potential in the modal dimension does not take obvious effect in our present discussion. In the previous section, we have chosen the parameters such as $\gamma = 0.01\,\mu\text{m}^{-1}$, $\delta = 0.005$, and $\lambda = 10\mu$m, leading to the ratio $\alpha = \delta\beta_0/\gamma \approx 40$, which means that the impact of on-site potential in the modal dimension is negligible with respect to the coupling coefficients of supermodes. In Fig. 4(a), we plot the conversion distance and the transformation rate η versus the perturbation coefficient α. The conversion distance increases with the perturbation coefficient and it is nearly a constant when α is big enough. However, the transformation rate is close to zero when α is equal to 1. It means that the linearly increasing on-site potential in the modal dimension plays a significant role in this condition. The conversion efficiency is in close proximity to 1 with the increase of the perturbation coefficient. In Fig. 4(b), we show the tracks of average modal intensity in modal space. The corresponding dynamics in the modal dimension are depicted in Figs. 4(c)–4(f). There is no efficient conversion of supermodes when γ is of the same order as $\delta\beta_0$. The linear on-site potential in the modal dimension suppresses the evolution of dynamics in modal space. By the way, it is obvious that there will be no coupling for supermodes in the absence of perturbation, which is derived from the applied gate voltage. Hence, the

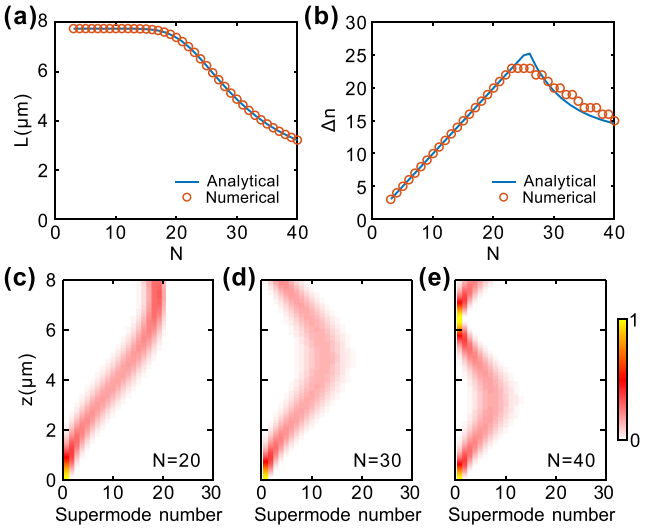

FIG. 5. Conversion distance of supermodes (a) and the amplitude of the mode variation (b) when the number of waveguides varies. (c)−(e) Dynamics of supermodes in modal space with the number of waveguides $N = 20$, 30, and 40 respectively.

conversion of supermodes can be controlled by switching on or off the applied voltage on graphene sheets.

To achieve the conversion of supermodes, we have considered a system with 13 waveguides to explore the characteristics of J_x lattices with linear modulation. In theory, it is proper for any number larger than 3 since at least two spaces between those waveguides could be variable, which does form a J_x array. Here we did not choose a very large number of waveguides because the modes in the system could be complicated and they are hard to excite and detect. For a J_x lattice with a larger number of waveguides, the distance between adjacent waveguides should decrease when the lateral size of the system is fixed. The reduction of spacing enhances the coupling and then results in the increase of γ, which is equivalent to increasing the ramp of on-site potentials in the modal dimension. As depicted in Fig. 5(a), the conversion distance of supermodes almost remains unchanged if $N \leqslant 15$. Then it decreases rapidly as the number of waveguides increases. The amplitude of the mode variation can be estimated by $\Delta n = 4\alpha\langle C_n\rangle/\gamma$ in theory. If $N \leqslant 25$, the value of γ is small so that $\Delta n > N$. Under this condition, the value of Δn should take the upper limit as N and the linear on-site potentials in the modal dimension do not take effect. As shown in Fig. 5(b), Δn decreases for larger mode numbers due to the increase of γ. The distributions of mode intensity during propagation for $N = 20$, 30, and 40 are shown in Figs. 5(c)–5(e). The conversion of supermodes is inhibited since the ramp of on-site potentials in the modal dimension increases. To achieve efficient conversion of supermodes, it should be suitable to choose a J_x waveguide array whose number is not so large.

So far, we have studied how the linear modulation amplitude of surface conductivity in J_x graphene waveguide arrays

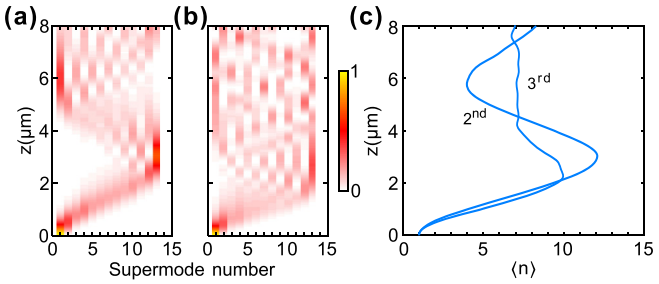

FIG. 6. (a),(b) Evolution of supermodes in modal space with (a) the second and (b) the third order nonlinear modulation. (c) Tracks of average modal intensity in modal space for the evolution of supermodes in (a) and (b).

acts on the conversion of supermodes. Here, we consider the second order nonlinear modulation of surface conductivity as $\Delta\sigma_g(n) = 0.001n^2\sigma_{g0}$ and the third order nonlinear modulation as $\Delta\sigma_g(n) = 0.0001n^3\sigma_{g0}$. The dynamics of supermodes for the second order and third nonlinear modulations are depicted in Figs. 6(a) and 6(b) respectively, and Fig. 6(c) shows the tracks of average modal intensity for the corresponding nonlinear modulations. It can be seen that the nonlinear modulation breaks the efficient conversion of supermodes. The stronger the nonlinearity is, the more chaotic dynamics of supermodes are. The influence of nonlinear modulation is prominently distinct from the linear modulation, since the latter results in the elegant transformation of Hamiltonian from real space to modal space. Hence, the efficient conversion of supermodes can only be realized in the case of linear modulation in J_x graphene waveguide arrays.

V. CONCLUSION

In summary, we construct a tunable supermode converter utilizing transversely modulated J_x graphene waveguide arrays. By linearly increasing the surface conductivity of graphene, we build a synthetic J_x lattice with linearly varying on-site potential in the modal dimension. As a result, any supermode can efficiently convert to its corresponding symmetric partner. The transformation rate is extremely high when the modulation ramp is much larger than the spacing of the eigenspectrum for the J_x lattice in real space. In this condition, the conversion distance of supermodes is inversely proportional to the ramp of linear modulation. The construction of the tunable supermode converter paves the way for the realization of mode converters and Mode-division multiplexing applications in optoelectronic devices.

ACKNOWLEDGMENTS

This work was supported by the National Natural Science Foundation of China (Grants No. 12374305, No. 11974124, No. 12021004, No. 12147151, and No. 12204185).

[1] M. Jablan, H. Buljan, and M. Soljačić, Plasmonics in graphene at infrared frequencies, Phys. Rev. B **80**, 245435 (2009).

[2] Q. Bao and K. P. Loh, Graphene photonics, plasmonics, and broadband optoelectronic devices, ACS Nano **6**, 3677 (2012).

[3] J. Christensen, A. Manjavacas, S. Thongrattanasiri, F. H. L. Koppens, and F. J. García De Abajo, Graphene plasmon waveguiding and hybridization in individual and paired nanoribbons, ACS Nano **6**, 431 (2012).
[4] Y. Fan, B. Wang, H. Huang, K. Wang, H. Long, and P. Lu, Plasmonic bloch oscillations in monolayer graphene sheet arrays, Opt. Lett. **39**, 6827 (2014).
[5] Y. Fan, B. Wang, K. Wang, H. Long, and P. Lu, Talbot effect in weakly coupled monolayer graphene sheet arrays, Opt. Lett. **39**, 3371 (2014).
[6] Y. Xu and H. Deng, Tunable anderson localization in disorder graphene sheet arrays, Opt. Lett. **41**, 567 (2016).
[7] Z. Hui Chen, Q. Long Tan, J. Lao, Y. Liang, and X. Guang Huang, Reconfigurable and tunable flat graphene photonic crystal circuits, Nanoscale **7**, 10912 (2015).
[8] C. Qin, B. Wang, H. Huang, H. Long, K. Wang, and P. Lu, Low-loss plasmonic supermodes in graphene multilayers, Opt. Express **22**, 25324 (2014).
[9] H. M. Price, T. Ozawa, and N. Goldman, Synthetic dimensions for cold atoms from shaking a harmonic trap, Phys. Rev. A **95**, 023607 (2017).
[10] Q. Lin, M. Xiao, L. Yuan, and S. Fan, Photonic weyl point in a two-dimensional resonator lattice with a synthetic frequency dimension, Nat. Commun. **7**, 13731 (2016).
[11] Q. Lin, X.-Q. Sun, M. Xiao, S.-C. Zhang, and S. Fan, A three-dimensional photonic topological insulator using a two-dimensional ring resonator lattice with a synthetic frequency dimension, Sci. Adv. **4**, eaat2774 (2018).
[12] E. Lustig, S. Weimann, Y. Plotnik, Y. Lumer, M. A. Bandres, A. Szameit, and M. Segev, Photonic topological insulator in synthetic dimensions, Nature (London) **567**, 356 (2019).
[13] A. Perez-Leija, R. Keil, H. Moya-Cessa, A. Szameit, and D. N. Christodoulides, Perfect transfer of path-entangled photons in J x photonic lattices, Phys. Rev. A **87**, 022303 (2013).
[14] J. Feldmann, K. Leo, J. Shah, D. A. B. Miller, J. E. Cunningham, T. Meier, G. Von Plessen, A. Schulze, P. Thomas, and S. Schmitt-Rink, Optical investigation of bloch oscillations in a semiconductor superlattice, Phys. Rev. B **46**, 7252 (1992).
[15] M. B. Dahan, E. Peik, J. Reichel, Y. Castin, and C. Salomon, Bloch oscillations of atoms in an optical potential, Phys. Rev. Lett. **76**, 4508 (1996).
[16] U. Peschel, T. Pertsch, and F. Lederer, Optical bloch oscillations in waveguide arrays, Opt. Lett. **23**, 1701 (1998).
[17] T. Pertsch, P. Dannberg, W. Elflein, A. Bräuer, and F. Lederer, Optical bloch oscillations in temperature tuned waveguide arrays, Phys. Rev. Lett. **83**, 4752 (1999).
[18] R. Morandotti, U. Peschel, J. S. Aitchison, H. S. Eisenberg, and Y. Silberberg, Experimental observation of linear and nonlinear optical bloch oscillations, Phys. Rev. Lett. **83**, 4756 (1999).
[19] G. C. Stey and G. Gusman, Wannier-stark ladders and the energy spectrum of an electron in a finite one dimensional crystal, J. Phys. C: Solid State Phys. **6**, 650 (1973).
[20] M. H. Teimourpour, D. N. Christodoulides, and R. El-Ganainy, Optical revivals in nonuniform supersymmetric photonic arrays, Opt. Lett. **41**, 372 (2016).
[21] M. Kuznetsov, Coupled wave analysis of multiple waveguide systems: The discrete harmonic oscillator, IEEE J. Quantum Electron. **21**, 1893 (1985).
[22] C. Du, G. Wang, Y. Zhang, and J.-H. Wu, Light transfer transitions beyond higher-order exceptional points in parity-time and anti-parity-time symmetric waveguide arrays, Opt. Express **30**, 20088 (2022).
[23] M. Christandl, N. Datta, A. Ekert, and A. J. Landahl, Perfect state transfer in quantum spin networks, Phys. Rev. Lett. **92**, 187902 (2004).
[24] X. Z. Zhang, L. Jin, and Z. Song, Perfect state transfer in PT -symmetric non-hermitian networks, Phys. Rev. A **85**, 012106 (2012).
[25] S. Weimann, A. Perez-Leija, M. Lebugle, R. Keil, M. Tichy, M. Gräfe, R. Heilmann, S. Nolte, H. Moya-Cessa, G. Weihs, D. N. Christodoulides, and A. Szameit, Implementation of quantum and classical discrete fractional fourier transforms, Nat. Commun. **7**, 11027 (2016).
[26] M. Bellec, G. M. Nikolopoulos, and S. Tzortzakis, Faithful communication hamiltonian in photonic lattices, Opt. Lett. **37**, 4504 (2012).
[27] A. Perez-Leija, R. Keil, A. Kay, H. Moya-Cessa, S. Nolte, L.-C. Kwek, B. M. Rodríguez-Lara, A. Szameit, and D. N. Christodoulides, Coherent quantum transport in photonic lattices, Phys. Rev. A **87**, 012309 (2013).
[28] K. Tschernig, R. D. J. León-Montiel, O. S. Magaña-Loaiza, A. Szameit, K. Busch, and A. Perez-Leija, Multiphoton discrete fractional fourier dynamics in waveguide beam splitters, J. Opt. Soc. Am. B **35**, 1985 (2018).
[29] K. Tschernig, R. De J. León-Montiel, A. Pérez-Leija, and K. Busch, Multiphoton synthetic lattices in multiport waveguide arrays: Synthetic atoms and fock graphs, Photon. Res. **8**, 1161 (2020).
[30] L. Ji, H. Zheng, A. Ismach, Z. Tan, S. Xun, E. Lin, V. Battaglia, V. Srinivasan, and Y. Zhang, Graphene/Si multilayer structure anodes for advanced half and full lithium-ion cells, Nano Energy **1**, 164 (2012).
[31] B. Wang, X. Zhang, K. Ping Loh, and J. Teng, Tunable broadband transmission and phase modulation of light through graphene multilayers, J. Appl. Phys. **115**, 213102 (2014).
[32] G. W. Hanson, Dyadic green's functions and guided surface waves for a surface conductivity model of graphene, J. Appl. Phys. **103**, 064302 (2008).
[33] D. A. Smirnova, I. V. Shadrivov, A. I. Smirnov, and Y. S. Kivshar, Dissipative plasmon-solitons in multilayer graphene: Dissipative plasmon-solitons in multilayer graphene, Laser Photon. Rev. **8**, 291 (2014).
[34] B. Wang, X. Zhang, F. J. García-Vidal, X. Yuan, and J. Teng, Strong coupling of surface plasmon polaritons in monolayer graphene sheet arrays, Phys. Rev. Lett. **109**, 073901 (2012).
[35] R. Yu, R. Alaee, F. Lederer, and C. Rockstuhl, Manipulating the interaction between localized and delocalized surface plasmon-polaritons in graphene, Phys. Rev. B **90**, 085409 (2014).
[36] P. Kang, K.-H. Kim, H.-G. Park, and S. Nam, Mechanically reconfigurable architectured graphene for tunable plasmonic resonances, Light Sci. Appl. **7**, 17 (2018).